JOURNAL OF PROPULSION AND POWER
Vol. 12, No. 2, March–April 1996

Vibration Signature Analysis of a Faulted Gear Transmission System

F. K. Choy* and S. Huang†
University of Akron, Akron, Ohio 44325
J. J. Zakrajsek‡
NASA Lewis Research Center, Cleveland, Ohio 44135
R. F. Handschuh§
U.S. Army Aviation Systems Command and NASA Lewis Research Center, Cleveland, Ohio 44135
and
D. P. Townsend¶
NASA Lewis Research Center, Cleveland, Ohio 44135

A comprehensive procedure in predicting faults in gear transmission systems under normal operating conditions is presented. Experimental data were obtained from a spiral bevel gear fatigue test rig at NASA Lewis Research Center. Time-synchronous-averaged vibration data were recorded throughout the test as the fault progressed from a small single pit to severe pitting over several teeth, and finally tooth fracture. A numerical procedure based on the Wigner–Ville distribution was used to examine the time-averaged vibration data. Results from the Wigner–Ville procedure are compared to results from a variety of signal analysis techniques that include time-domain analysis methods and frequency analysis methods. Using photographs of the gear tooth at various stages of damage, the limitations and accuracy of the various techniques are compared and discussed. Conclusions are drawn from the comparison of the different approaches as well as the applicability of the Wigner–Ville method in predicting gear faults.

I. Introduction

IN the last two decades, with the ever increasing demand for higher power and performance, premature failures in high-performance machinery often result in major production and financial losses, and sometimes even lead to catastrophic consequences. In the aerospace industry, one of the major concerns is the rotorcraft transmission system. Currently, on-board operational condition monitoring systems for rotorcraft transmissions often fail to provide sufficient time between warning and failure so that safety procedures can be implemented. In addition, inaccurate interpretation of operating conditions often result in false alarms and unnecessary repairs and downtime. The development of an accurate machine health monitoring system for rotorcraft transmission systems will increase safety and reduce financial investments.

The objective of this article is to examine and compare the three different approaches to detect gear wear and failure. The frequency-domain analysis is based on the spectral display from a fast Fourier transform (FFT) algorithm. The time-domain analysis includes the time-synchronous-averaged signal and the statistical-based techniques FM0, FM4, NA4*, and NB4* applied to the time-averaged signal. The joint time-frequency analysis uses the Wigner–Ville distribution (WVD) on the vibration data with special windowing techniques. All of the analysis methods are applied to the vibration data of a failure from the spiral bevel gear fatigue test rig in the NASA Lewis Research Center. Results from the various methods are compared and general conclusions are drawn from the results.

Presented as Paper 94-2937 at the AIAA/ASME/SAE/ASEE 30th Joint Propulsion Conference and Exhibit, Indianapolis, IN, June 27–29, 1994; received July 5, 1994; revision received Sept. 1, 1995; accepted for publication Sept. 12, 1995.

*Professor, Department of Mechanical Engineering.
†Graduate Student, Department of Mechanical Engineering.
‡Research Engineer, Aerospace Directorate.
§Aerospace Engineer, Propulsion Directorate.
¶Senior Research Engineer, Aerospace Directorate.

II. Technical Approach

As discussed in the previous section, three major methodologies, 1) the frequency domain approach, 2) the time-domain approach, and 3) the joint time-frequency approach are used in this study. The following is a description of the three methodologies:

A. Frequency Domain Techniques

The frequency spectrum is found by applying a discrete FFT on the time-averaged signal $x(t)$, such that the spectral components are

$$X(k) = T \sum_{i=0}^{N-1} x(t) \exp\left(\frac{-j2\pi ik}{N}\right) \tag{1}$$

where $x(t)$ is the time domain signal, $X(k)$ is the frequency domain signal, T is the sampling time interval, and N is the number of data points. The frequency components are examined in the frequency domain and compared with those obtained at various stages of the fault development in the spiral bevel pinion.

B. Time-Domain Techniques

Four different time domain techniques for early detection of gear tooth damage are used in this study for evaluation and comparison. All of the time-domain techniques are applied to the vibration signal after it has been time-synchronously averaged. These techniques are FM0, FM4, NA4*, and NB4*. These parameters are defined as follows:

FM0[1] is a course fault detection parameter that compares the maximum peak-to-peak amplitude to the sum of the mesh frequencies and its harmonics

$$\text{FM0} = PP \Big/ \sum_{i=1}^{n} A(f_i) \tag{2}$$

where PP is the maximum peak-to-peak amplitude in signal, $A(f_i)$ is the amplitude at mesh frequency and harmonics, n is the total number of harmonics in frequency range, and FM4[1] is an isolated fault detection parameter, and is given by the normalized kurtosis of the resulting difference signal as

$$\text{FM4} = N \sum_{i=1}^{N} (d_i - \bar{d})^4 \Big/ \left[\sum_{i=1}^{N} (d_i - \bar{d})^2 \right]^2 \tag{3}$$

where $d(t) = A(t) - R(t)$, $\bar{d}$ is the mean value of $d(t)$, $A(t)$ is the original time synchronous signal, $R(t)$ is the regular meshing components plus their first-order sidebands, and N is the total number of data points in the time signal.

NA4* (Refs. 2–4) is a general fault detection parameter with trending capabilities. A residual signal is constructed by removing regular meshing components from the time-averaged signal. For NA4, the first-order sidebands stay in the residual signal and the fourth statistical moment of the residual signal is then divided by the averaged variance of the residual signal, raised to the second power. The average variance is the mean value of the variance of all previous records in the run ensemble. This allows NA4 to compare the current gear vibration with the baseline of the system under nominal conditions. NA4 is given by the quasinormalized kurtosis equation shown next:

$$\text{NA4*}(M) = N \sum_{i=1}^{N} (r_i - \bar{r})^4 \Big/ \left\{ \frac{1}{M} \sum_{j=1}^{N} \left[\sum_{i=1}^{N} (r_{ij} - \bar{r}_j)^2 \right] \right\}^2 \tag{4}$$

where r is the residual signal, $\bar{r}$ is the mean value of residual signal, N is the total number of data points, in one time record, i is the data point number in time record, j is the time record number, and M is the current time record number in run ensemble.

An enhancement to this parameter is given by NA4*, in which the value of the averaged variance is locked when the instantaneous variance exceeds a predetermined value.[2] This provides NA4 with enhanced trending capabilities, in which the kurtosis of the current signal is compared to the variance of the locked baseline signal under nominal conditions.

NB4 is another parameter similar to NA4 that also uses the quasinormalized kurtosis given in Eq. (4). The major difference is that instead of using a residual signal, NB4 uses the envelope of the signal bandpassed about the mesh frequency. Again, as with NA4*, NB4* is an enhancement to the NB4 parameter, in which the value of the average variance is locked when the instantaneous variance exceeds a predetermined value. The equation for NB4* is given as follows:

$$\text{NB4*}(M) = N \sum_{i=1}^{N} (s_i - \bar{s})^4 \Big/ \left\{ \frac{1}{M} \sum_{j=1}^{N} \left[\sum_{i=1}^{N} (s_{ij} - \bar{s}_j)^2 \right] \right\}^2 \tag{5}$$

$$s(t) = \text{magnitude of } (b(t) + i\{H[b(t)]\}) \tag{6}$$

where $b(t)$ is the time-averaged signal bandpassed filtered about the meshing frequency, $H[b(t)]$ is the Hilbert Transform of $b(t)$, N is the total number of data points in one time record, i is the data point number in time record, j is the time record number, and M is the current time record number in run ensemble.

C. Joint Time-Frequency Technique

To examine the vibration signal in a joint time-frequency domain, the Wigner–Ville method[5–11] is used in this study. While the FFT technique [Eq. (1)] can provide the spectral contents of the time signal, it cannot distinguish time phase change during a complete cycle of operation. In other words, it assumes that the time signals are repeatable for each time data acquisition window without considering the effects of any magnitude and phase changes during the sampling period. The Wigner–Ville distribution will provide an interactive relationship between time and frequency during the period of the time data window. The WVD can be written as

$$W(t, f) = \sum_{-\infty}^{\infty} x\left(t + \frac{\tau}{2}\right) x^*\left(t - \frac{\tau}{2}\right) e^{-j2\pi f\tau} \, d\tau \tag{7}$$

To allow sampling at the Nyquist rate and eliminate the concentration of energy around the frequency origin because of the cross product between negative and positive frequency,[5,7] the analytic signal was used in evaluating the WVD. The analytic signal $s(t)$ is defined as

$$s(t) = x(t) + jH[x(t)] \tag{8}$$

where $H[x(t)]$ is the Hilbert transform of $x(t)$ defined by

$$H[x(t)] = \frac{1}{\pi} \int_{-\infty}^{\infty} \frac{x(\xi)}{t - \xi} \, d\xi \tag{9}$$

However, an alternative approach can be used to calculate the analytic signal using the frequency domain definition. The analytic signal $s(t)$ can be evaluated by calculating the FFT of the time signal $x(t)$, then setting the negative frequency spectrum to zero. The analytic signal can be obtained by evaluating the inverse FFT of the spectrum. To simplify the computational effort, the WVD can be evaluated using a standard FFT algorithm. Adopting the convention that the sampling period is normalized to unity, Eq. (7) can be rewritten as

$$W_x(n, f) = 2 \sum_{i=-L}^{L} x(n + i)x^*(n - i) \cdot e^{-j4\pi fi} \tag{10}$$

As for the continuous time case, it is necessary only to evaluate the WVD at time zero. Hence,

$$W_x(0, f) = 2 \sum_{i=-L}^{L} k(i) e^{-j4\pi fi} \tag{11}$$

where $k(i) = s(i)s^*(-i)$. Equation (12) can be evaluated using the discrete FFT algorithm.

To avoid a repetition in the time-domain WVD, a weighting function[10] is added to the time data before the evaluation process. Such a process may decrease the resolution of the distribution, but it will eliminate the repetition of peaks in the time domain and the interpretation of the result will be substantially easier.

III. Description of Experimental Procedure

The fatigue damage on the test pinion shown in Figs. 1–8 was obtained using the spiral bevel gear fatigue test rig, illustrated in Fig. 9, at the NASA Lewis Research Center. The primary purpose of this rig is to study the effects of gear tooth design, gear materials, and lubrication types on the fatigue strength of aircraft quality gears.[12] Because spiral bevel gears are used extensively in helicopter transmissions to transfer power between nonparallel intersecting shafts, the use of this fatigue rig for diagnostic studies is extremely practical. Vibration data from an accelerometer mounted on the pinion shaft bearing housing was captured using a personal computer with an analog-to-digital conversion board and antialiasing filter. The 12-tooth test pinion, and the 36-tooth gear have 0.5141 in pitch, 35-deg spiral angle, 1-in. face width, 90-deg shaft angle,

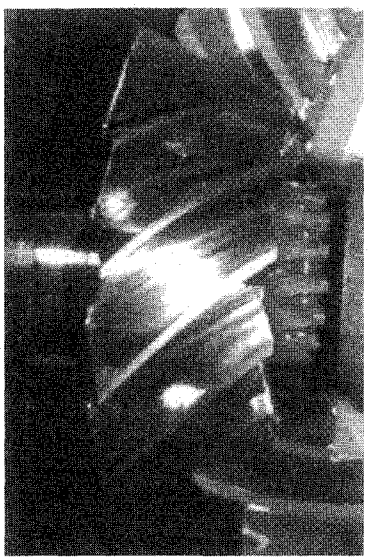

Fig. 1 Photograph of pinion at t = 5.50 h.

Fig. 2 Photograph of pinion damage at t = 6.55 h.

Fig. 3 Photograph of pinion damage at t = 8.55 h.

Fig. 4 Photograph of pinion damage at t = 10.03 h.

Fig. 5 Photograph of pinion damage at t = 12.03 h.

Fig. 6 Photograph of pinion damage at t = 14.53 h.

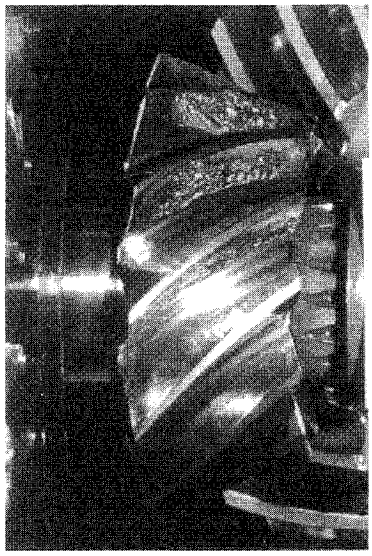

Fig. 7 Photograph of pinion damage at t = 16.16 h.

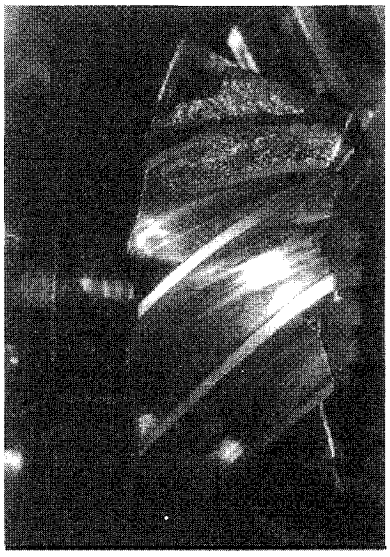

Fig. 8 Photograph of pinion damage at t = 17.79 h (end of run).

and 22.5-deg pressure angle. The pinion transmits 720 hp at a nominal speed of 14,400 rpm. The test rig was started and stopped several times for gear damage inspection. The test was ended at 17.79 operational hours when a broken portion of a tooth was found visually during one of the shutdowns.

IV. Discussions of Results

A series of photographs showing the deterioration of the pinion teeth at various stages of the test is illustrated in Figs. 1–8. In Fig. 1 the initiation of a small pit on one of the pinion teeth during the first shutdown, at about $5\frac{1}{2}$ h into the test is shown. As the test progressed, the rig was shut down seven more times to examine the severity of the pitting and its relationship with the corresponding vibrations. Figures 2–4 show the increase of the damaged area at the pinion tooth as the elapsed time increased to 6.55, 8.55, and 10.03 h, respectively. Note that in Fig. 5, as the elapsed time increased to 12 h, the damage of the pinion tooth increased to 75% of the tooth surface. At this stage, pitting also initiated on the adjacent tooth and continued to grow as the time increased to 14.53 h, Fig. 6. At 16.16 h, the damage had grown to three adjacent teeth as shown in Fig. 7. The test was terminated when a breakage was detected on one of the three heavily pitted teeth at 17.79 h, as shown in Fig. 8.

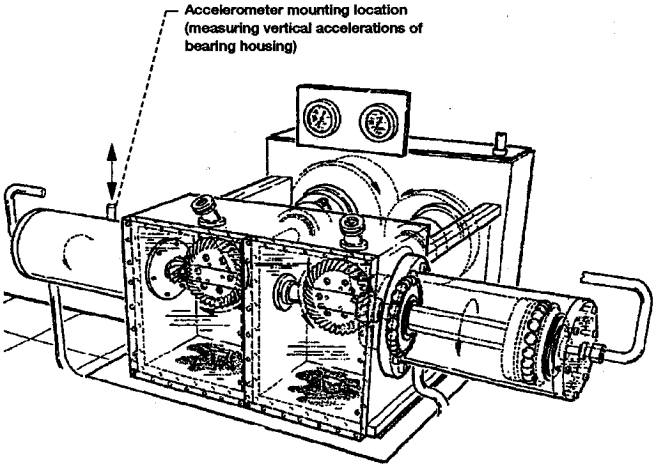

Fig. 9 Spiral bevel gear test rig at NASA Lewis Research Center.

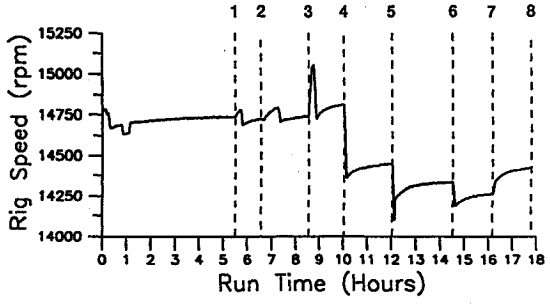

Fig. 10 Rig operating speed at various run times.

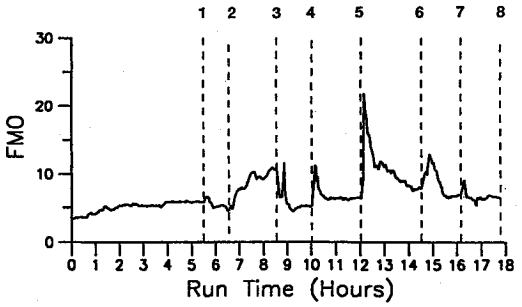

Fig. 11 FM0 parameter at various run times.

Figure 10 depicts the running speed of the test rig during various stages of the experiment. Note that there ares some fluctuations present in the running speed after each shutdown, with a magnitude of approximately 6% about the nominal pinion speed of 14,400 rpm. There is a sharp change in speed at approximately 8.75 h. These variations in speed create a substantial effect on the vibration signal, which is amplified in the NA4, NB4, and the WVD analysis.

Figure 11 shows the results of the FM0 analysis. As seen from the figure, FM0 shows only moderate changes as the damage starts and progresses. It does not provide any indication of further damages as pittings extend to the adjacent teeth, resulting in pinion tooth fracture. The majority of the variations in the FM0 parameter are most probably because of the speed changes experienced during the test.

Results from the FM4 parameter, as seen in Fig. 12, show a possible reaction as the pitting started to occur, however, it does not provide any coherent indication of the severity of the pitting as the damage increased. In addition, it does not provide any information to distinguish the pitting of single or multiple teeth.

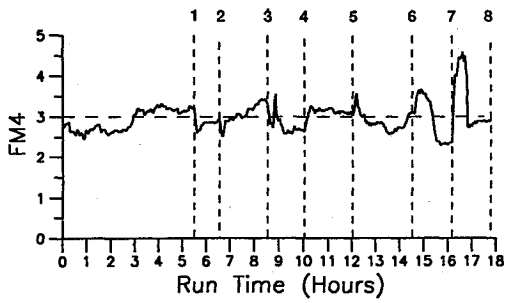

Fig. 12 FM4 parameter at various run times.

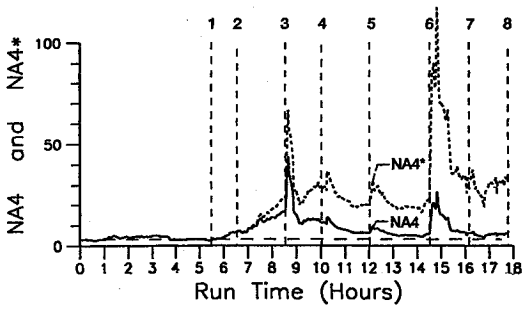

Fig. 13 NA4 and NA4* at various run times.

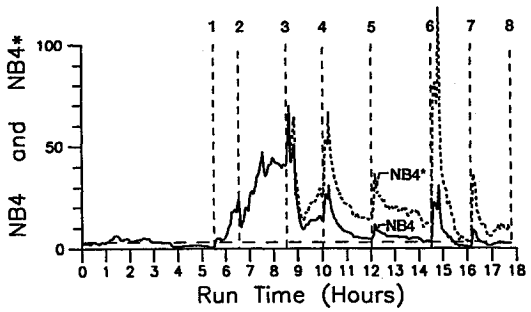

Fig. 14 NB4 and NB4* at various run times.

Results from NA4 and NA4* are illustrated in Fig. 13. It is obvious from the figure that both NA4 and NA4* provide a very good indication of the pitting development on the pinion tooth. The magnitude of the parameter increases to a nondimensional value of 7 after shutdown no. 2 at 6.55 h, and further to a value of 17 when the pitting covers 75% of the tooth surface at 8.5 h. As expected, the locked denominator in NA4* provides a more robust indication as the pitting progresses.[2,4] Again, both parameters are very sensitive to the speed variations, especially after shutdown nos. 3 and 6.

The NB4 and NB4* parameters, as shown in Fig. 14, show a very similar trend to those of NA4 and NA4*, with a more robust indication to the severity of the damage. However, both NA4 and NB4 did not provide any type of indication as the damage spread to other teeth, and finally, as tooth fracture occurred.

Figure 15 shows the WVD (and corresponding intensity scale) and (below the WVD) the frequency spectrum (from FFT analysis) of the uniform sine wave signal shown at the left side of the figure. Note that only the frequency component of the input frequency is detected by both the frequency domain analysis and the joint time-frequency distribution. The WVD does not exhibit any changes during the 1 cycle (0–360 deg) rotation of the shaft. When a short-term amplitude and phase change is added to the system, as shown in Fig. 16, the frequency spectrum remains virtually unchanged. The WVD shows a dramatic change of the energy distribution pattern at the location where the change occurs. The lighter shades of the distribution display indicate a smaller vibration amplitude, which is shown by the time signal at the left side of the figure.

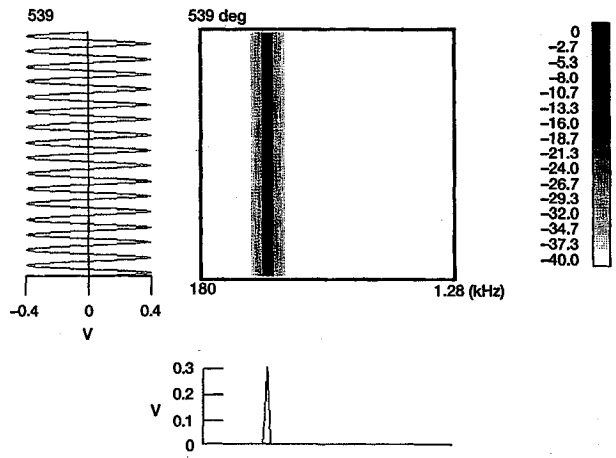

Fig. 15 Example of WVD on a regular sine wave time signal.

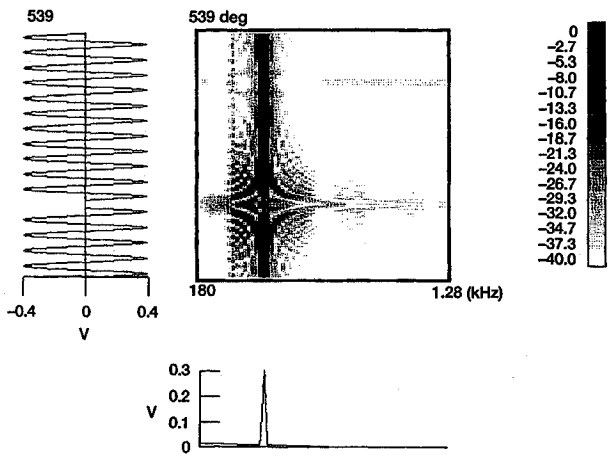

Fig. 16 Example of WVD on short-term amplitude and phase change in a signal.

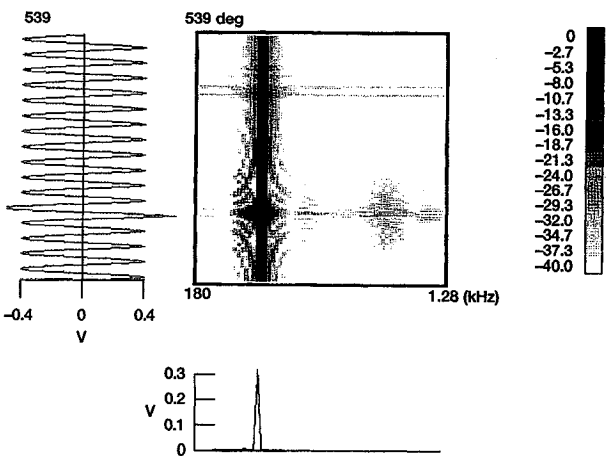

Fig. 17 Example of WVD on short-term amplitude increase in a signal.

Such an effect could possibly be caused by a chipped or cracked tooth. Figure 17 shows the effects of a short-term amplitude increase in the time signal to simulate vibrations caused by gear tooth surface damage. Note that the frequency spectrum remains the same showing only the component of the exciting frequency, whereas the WVD again provides a good indication of the amplitude increase by the widening of the shaded area to a diamond shape at the corresponding damaged tooth location. Figure 18 shows the effects of a time-decaying short-term amplitude and phase-change signal. The WVD

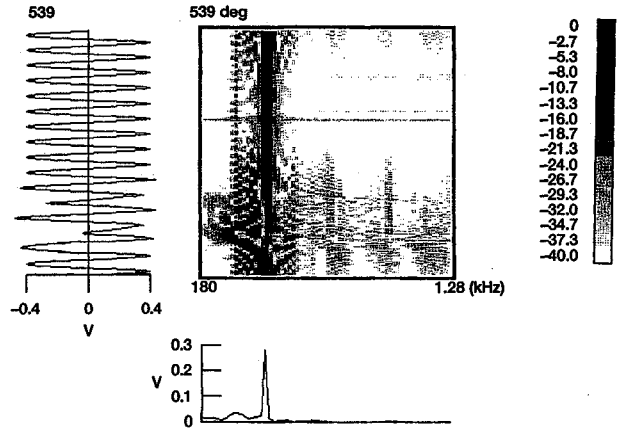

Fig. 18 Example of WVD on time decay of a short-term amplitude and phase change in a signal.

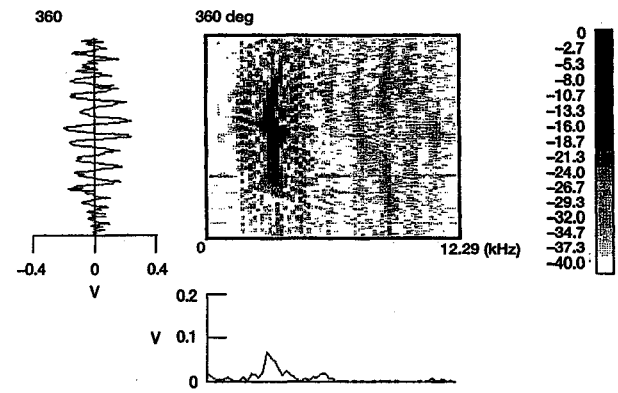

Fig. 19 Application of WVD to the spiral bevel gear vibration signal at 5.50 h.

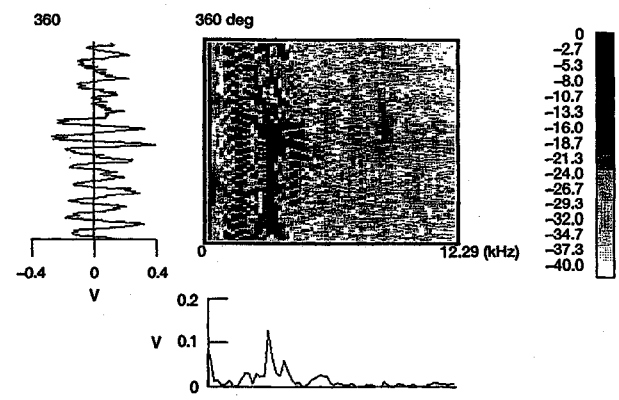

Fig. 20 Application of WVD to the spiral bevel gear vibration signal at 6.55 h.

shows a half diamond shape of shaded area, similar to that of Fig. 16, at the location where the amplitude and phase changes are presented. As seen in Fig. 18, the frequency spectrum gives very little indication of the signal change.

Figures 19–26 show the WVD and frequency spectra of the spiral bevel pinion vibration at various stages of damage, corresponding to the photographs given in Figs. 1–8. Figure 19 shows the occurrence of the initial pitting at around 200 deg from the triggering point of the gear at 5.5 h of running time. At 6.55 h, the pitting on the tooth surface progressed to a more noticeable stage, as shown in Fig. 2, and the WVD pattern (Fig. 20), begins to adopt those of a short-term amplitude and phase change as illustrated in Fig. 18. At this stage, a Cross pattern appeared in the joint time-frequency domain (WVD) as the damaged gear tooth produced a change in the frequency

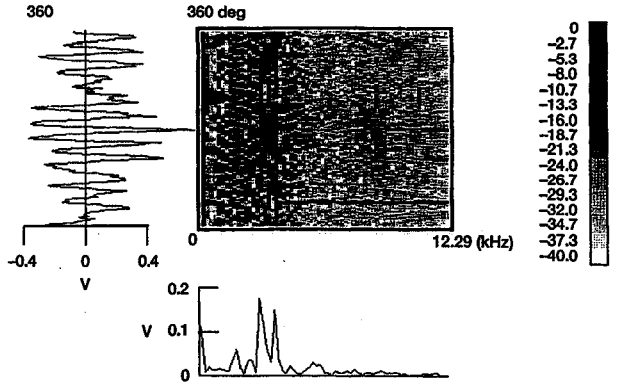

Fig. 21 Application of WVD to the spiral bevel gear vibration signal at 8.55 h.

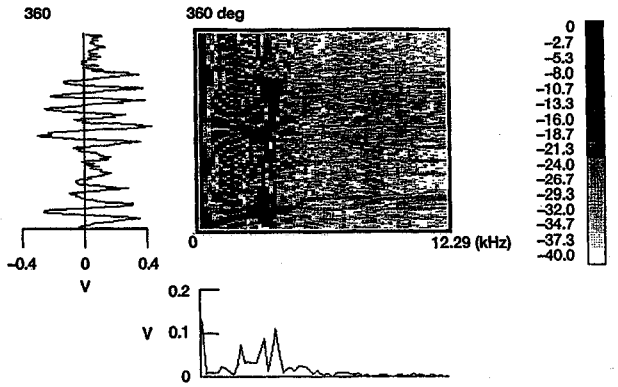

Fig. 22 Application of WVD to the spiral bevel gear vibration signal at 10.03 h.

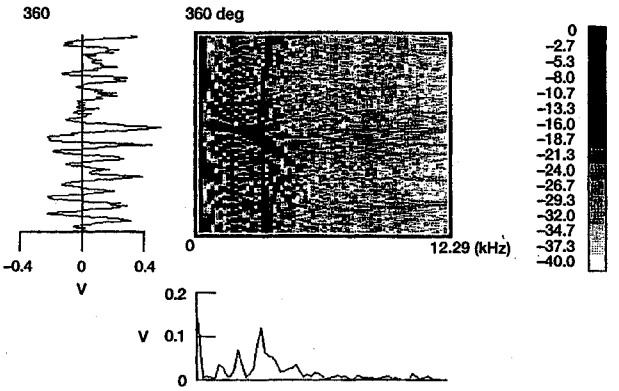

Fig. 23 Application of WVD to the spiral bevel gear vibration signal at 12.03 h.

components other than the mesh frequency. Because of the speed increase at 8.55 h, the overall WVD amplitude increases substantially as shown in Fig. 21. At the running time of 10.03 h, the corresponding WVD in Fig. 22 shows the initiation of a cross pattern as surface pitting in the damaged tooth becomes more pronounced, which can also be evidenced from the photograph of the pinion gear in Fig. 4. This phenomenon is also evident in the frequency spectrum with the existence of sideband components. At 12.03 h, when the pitting on the pinion tooth has extended to about 75% of the tooth surface as shown in Fig. 5, the WVD pattern exhibits a solid cross pattern extending over the mesh frequency and several of its adjacent sidebands. The high concentration in the WVD energy and the initiation of a second cross pattern at 14.53 h (Fig. 24), show the advancement of the pitting process on a second tooth, as illustrated in Fig. 6. This is further confirmed by the large

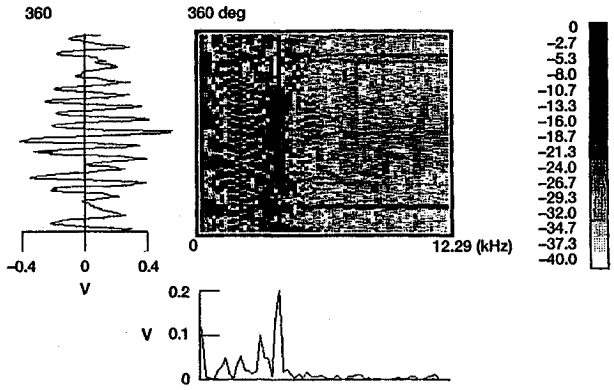

Fig. 24 Application of WVD to the spiral bevel gear vibration signal at 14.53 h.

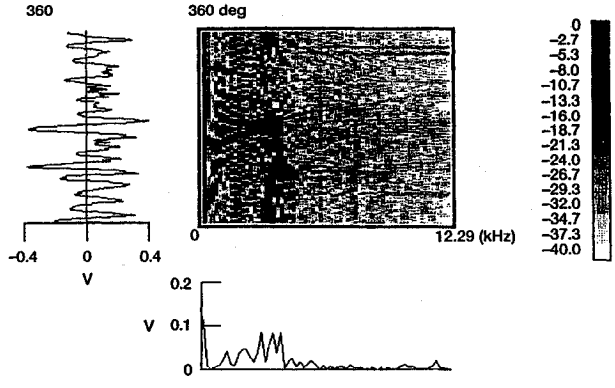

Fig. 25 Application of WVD to the spiral bevel gear vibration signal at 16.16 h.

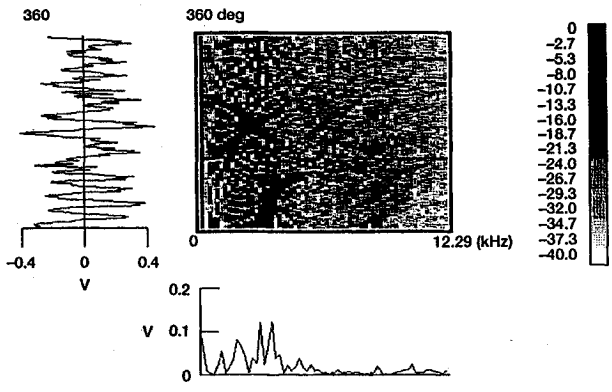

Fig. 26 Application of WVD to the spiral bevel gear vibration signal at 17.79 h.

amplitude of a sideband component (above mesh) in the frequency spectrum. At 16.16 h, as seen in Fig. 25, the WVD pattern changes, showing a more advanced damage pattern similar to the multiples of the decay of a single short-term amplitude increase and phase change demonstrated in Fig. 18. Such phenomenon is because of the pitting of three consecutive teeth in the pinion gear as shown in the photograph given in Fig. 7. The frequency spectrum in Fig. 25 shows a substantial amplitude increase in the sideband components. The discontinuity of the WVD at the mesh frequency, shown in Fig. 26, similar to the example shown in Fig. 16 because of the short-term phase change, is probably the result of the instantaneous phase change caused by the fractured tooth, as illustrated in Fig. 8. The two cross patterns in the WVD are very distinct as the effects of pitting at the teeth adjacent to the fracture tooth become more pronounced. Note, also that, as given in Fig. 26, the amplitude of the sideband frequencies (above and below the mesh frequency) increase substantially.

V. Conclusions

Based on the results of the application of the various aforementioned methods, the following conclusions can be made:

1) The FM0 parameter shows only moderate changes as the damage starts and progresses. It also fails to indicate the fracture of the pinion tooth.

2) The FM4 parameter shows a possible reaction to the start of the pitting process, however, no coherent indication is provided for the growth and severity of the pit.

3) The NA4* and NB4* parameters show good reactions to the initial pitting damage and very nice indications for the growth and severity of the pitting damage. However, their indications for the tooth fracture are somewhat unclear.

4) The WVD provides vital information concerning both the severity and the location of the pitting process in the gear system.

5) The fracture of the gear tooth and its exact location can be pinpointed using the WVD technique. However, a machine vibration signature database is required to interpret the resulting WVD.

6) The occurrence and the severity of gear tooth failure can be reliably detected using a combination of time averaging, frequency analysis, and WVD techniques.

References

[1]Stewart, R. M., "Some Useful Data Analysis Techniques for Gearbox Diagnostics," Inst. of Sound and Vibration Research, Paper MHM/R/10/77, July 1977.

[2]Decker, H. J., Handschuh, R. F., and Zakrajsek, J. J., "An Enhancement to the NAU Gear Vibration Diagnostic Parameter," NASA TM-106553, June 1994.

[3]Zakrajsek, J. J., Towsend, D. P., and Decker, H. J., "An Analysis of Gear Fault Detection Methods as Applied to Pitting Fatigue Failure Data," NASA TM-105950, April 1993.

[4]Zakrajsek, J. J., Handschuh, R. F., and Decker, H. J., "Application of Fault Detection Techniques to Spiral Bevel Gear Fatigue Data," NASA TM-106467, April 1994.

[5]Boashash, B., and Black, P. J., "An Efficient Real-Time Implementation of the Wigner-Ville Distribution," *IEEE Transactions on Acoustics, Speech, and Signal Processing*, Vol. ASSP-35, No. 11, 1987, pp. 1611–1618.

[6]Bouachache, B., and Flandrin, P., "Wigner-Ville Analysis of Time-Varying Signals," *Proceedings of the ICASSP* (Paris, France), 1982, pp. 1329–1333.

[7]Claasen, T. A. C. M., and Mecklenbräuker, W. F. G., "The Wigner Distribution—A Tool for Time-Frequency Signal Analysis," *Philips Research Report*, Vol. 35, Pt. 1, 1980, pp. 373–389.

[8]Peyrin, F., and Prost, R., "A Uniform Definition for the Discrete-Time, Discrete-Frequency, and Discrete-Time/Frequency Wigner Distribution," *IEEE Transaction on Acoustics, Speech and Signal Processing*, Vol. ASS-34, No. 4, 1986, pp. 858–867.

[9]Forrester, B. D., "Analysis of Gear Vibration in the Time-Frequency Domain," *Proceedings of the 44th Meeting of the Mechanical Failure Prevention Group*, Cambridge Univ. Press, Cambridge, England, UK, 1990, pp. 225–234.

[10]Mcfadden, P. D., and Wang, W. J., "Time-Frequency Domain Analysis of Vibration Signal for Machinery Diagnostics (II) the Weighted Wigner-Ville Distribution," Univ. of Oxford, Rept. OUEL 1891, Oxford, England, UK, 1991.

[11]Shin, Y. S., and Jeon, J. J., "Pseudo Wigner-Ville Time-Frequency Distribution and Its Application to Machinery Condition Monitoring," *Journal of Shock and Vibration*, Vol. 1, No. 1, 1993, pp. 65–76.

[12]Handschuh, R., "Effect of Lubricant Jet Location on Spiral Bevel Gear Operating Temperatures," 6th International Power Transmission and Gearing Conf., American Society of Mechanical Engineers, Phoenix, AZ, Sept. 1992; also NASA TM-105656, AUSCOM TR-91-C-033.